Enhanced detection of a low-frequency signal by using broad squeezed light and a bichromatic local oscillator

Wei Li,[1,2] Yuanbin Jin,[1,2] Xudong Yu,[1,2] and Jing Zhang[1,3,*]

[1]*State Key Laboratory of Quantum Optics and Quantum Optics Devices, Institute of Opto-Electronics, Shanxi University, Taiyuan 030006, People's Republic of China*

[2]*Collaborative Innovation Center of Extreme Optics, Shanxi University, Taiyuan 030006, People's Republic of China*

[3]*Synergetic Innovation Center of Quantum Information and Quantum Physics, University of Science and Technology of China, Hefei, Anhui 230026, People's Republic of China*

(Received 12 March 2017; published 4 August 2017)

We experimentally study a protocol of using the broadband high-frequency squeezed vacuum to detect the low-frequency signal. In this scheme, the lower sideband field of the squeezed light carries the low-frequency modulation signal, and the two strong coherent light fields are applied as the bichromatic local oscillator in the homodyne detection to measure the quantum entanglement of the upper and lower sideband for the broadband squeezed light. The power of one of the local oscillators for detecting the upper sideband can be adjusted to optimize the conditional variance in the low-frequency regime by subtracting the photocurrent of the upper sideband field of the squeezed light from that of the lower sideband field. By means of the quantum correlation of the upper and lower sideband for the broadband squeezed light, the low-frequency signal beyond the standard quantum limit is measured. This scheme is appropriate for enhancing the sensitivity of the low-frequency signal by the aid of the broad squeezed light, such as gravitational waves detection, and does not need to directly produce the low-frequency squeezing in an optical parametric process.

DOI: 10.1103/PhysRevA.96.023808

The first detection of gravitational waves (GWs) emitted from the merger of two black holes by the Laser Interferometer Gravitational-Wave Observatory (LIGO) has set the course for a new era of astrophysics. GW detection is now opening an exciting new observational frontier in astronomy and cosmology [1–3]. The further improvement of GW detector sensitivity is expected to extend the detection range and the event rate of binary black holes coalescence and may lead to detections of more exotic sources.

In advanced LIGO, vacuum fluctuations entering from the dark port of the interferometer [4] can make the quadrature phase of the output carrier field at the dark port noisy, which contains a GW signal. However, as the squeezed vacuum state is fed into the dark port of the interferometer, the sensitivity can be improved beyond the standard quantum limit (SQL) [5,6]. The use of squeezed states to enhance the sensitivity began with initial proof-of-principle experiments and recently has been demonstrated by GEO 600 [7] and LIGO [8]. Since the terrestrial GW signal locates in the 10 Hz to 10 kHz band [9,10], squeezing in the audio band is required, which is a great technical challenge. Until now, there has been very wide research demonstrating squeezing at the lower frequency band [11–13] and applications in quantum metrology [14–24].

Broadband squeezing has been demonstrated at megahertz frequencies, where technical noise sources of the laser light are not present. At these frequencies, the laser operates at or near the shot-noise limit. Due to the strong quantum correlation between the lower and upper sideband of the squeezed light field, the single broadband squeezed light can be split into N pairs of upper and lower sideband fields with spatial separation to produce N independent Einstein-Podolsky-Rosen (EPR) entangled fields [25]. This scheme was demonstrated experimentally by using a pair of frequency-shifted local oscillators to measure this EPR entanglement [26,27]. Recently a theoretical protocol was proposed to improve LIGO's sensitivity beyond the SQL via EPR entanglement of the broad squeezing field and the dual use of the interferometer as both the GW detector and the filter, eliminating the need for external narrow filter cavities [28]. In this paper, we employ a broadband high-frequency squeezed vacuum to detect low-frequency signal beyond the standard quantum limit. The broadband squeezed vacuum consists of a pair of EPR entangled beams: the signal beam (lower sideband field) around the carrier frequency ω_0, and the idler beam (upper sideband field) around $\omega_0 + \Lambda$. The lower sideband field around the carrier frequency ω_0 will carry the low-frequency modulation signal around the carrier frequency ω_0; however, the upper sideband field around $\omega_0 + \Lambda$ feels nothing. The output lower and upper sideband fields may be separated in space by a mode cleaner cavity and measured by homodyne detection with two local oscillators at frequency ω_0 and $\omega_0 + \Lambda$, respectively. The conditional squeezing of the output signal beam can be obtained by subtracting the photocurrent of the idler beam from that of the signal beam. Here the lower and upper sideband fields of the broad squeezed light may be separated in space by a mode cleaner cavity before or after carrying the low-frequency modulation signal. Thus this scheme also can be considered as follows. (1) The broadband squeezed vacuum is separated into the lower and upper sideband fields in space by a mode cleaner cavity. (2) The lower sideband field around the carrier frequency ω_0 is sent into sensitive device (such as the interferometer); therefore, the low-frequency signal around the carrier frequency ω_0 is added in the lower sideband field by the sensitive device. (3) The lower and upper sideband fields are measured by homodyne detection with two local oscillators at frequency

*Corresponding author: jzhang74@sxu.edu.cn, jzhang74@yahoo.com

 ©2017 American Physical Society

ω_0 and $\omega_0 + \Lambda$, respectively. The conditional variance of the lower sideband beam can be obtained by subtracting the photocurrent of the upper sideband beam from that of the lower sideband beam. Thus this scheme can avoid producing the low-frequency squeezing to improve the sensitivity of the interferometer.

In this paper, we remove the mode cleaner cavity to separate the signal and idler beams in space and utilize a bichromatic local oscillator (BLO) to directly detect the signal and idler beams of a broad high-frequency squeezed vacuum after carrying the low-frequency signal by combining with a phase-modulated coherent light at around ω_0 on a beam splitter. This scheme can avoid optical losses introduced by the mode cleaner cavity. Moreover by optimally adjusting the power of one local oscillator for detecting the idler field, we can obtain the minimum conditional variance of the signal beam and improve the signal noise ratio. The theoretical scheme based on the BLO to detect the squeezed state was proposed in Ref. [29] and the phase-sensitive detection with a BLO or a double-sideband signal field was studied experimentally [30–32]. The measurement of a broad squeezed vacuum state by means of a BLO was demonstrated experimentally [33,34]. Recently, by making use of the multifrequency homodyne detection, the experiments of cross-frequency entanglements generated in periodically pumped optical parametric oscillators (OPOs) have been reported [35,36].

The schematic diagram of the detection is shown in Fig. 1(a). A BLO with two local oscillators at frequency ω_0 and $\omega_0 + \Lambda$ is mixed with the detected light field at a 50:50 beam splitter. The power of one local oscillator (upper local oscillator) at $\omega_0 + \Lambda$ can be adjusted with the factor g. The relative phase θ of the local oscillator and the detected field can be controlled by the reflective mirror mounted on a piezoelectric transducer (PZT). The annihilation operators of the BLO and the detected signal field can be written as $\hat{a}(t) = \hat{a}_-(t)\exp[-i\omega_0 t] + \hat{a}_+(t)\exp[-i(\omega_0 + \Lambda)t]$ and $\hat{b}(t) = \hat{b}_0(t)\exp(-i\omega_0 t)$, where $\hat{a}_{+(-)}(t)$ and $\hat{b}_0(t)$ are the slowly varying operators of the fields. The normalized difference of the photocurrents of the two detectors at the 50:50 beam splitter is

$$\hat{i}(t) = \frac{1}{a}[\langle\hat{a}^\dagger(t)\rangle\hat{b}(t)e^{-i\theta} + \langle\hat{a}(t)\rangle\hat{b}^\dagger(t)e^{i\theta}], \tag{1}$$

where the fields satisfy $\langle\hat{a}_+\rangle = ga$, and $\langle\hat{a}_-\rangle = a \gg \langle\hat{b}_0\rangle \sim 0$. Therefore the BLO is a pair of the strong coherent states, and the detected field is the vacuum state or the squeezed vacuum state carrying the low-frequency signal around frequency ω_0.

The difference of the photocurrents analyzed at the radio frequency Ω is expressed as

$$\hat{i}(\Omega) = \hat{Q}_-(\Omega,\theta) + g\hat{Q}_+(\Omega,\theta). \tag{2}$$

Here we express the quadrature component of the signal field around the central frequency ω_0, which easily compares with the measurement with a single local oscillator ($g = 0$) at ω_0. Therefore, the quadrature component of the detected field can be defined as $\hat{Q}_-(\Omega,\theta) = \hat{b}(\omega_0 - \Omega)e^{-i\theta} + \hat{b}^\dagger(\omega_0 + \Omega)e^{i\theta}$, and $\hat{Q}_+(\Omega,\theta) = \hat{b}(\omega_0 + \Lambda - \Omega)e^{-i\theta} + \hat{b}^\dagger(\omega_0 + \Lambda + \Omega)e^{i\theta}$. The quadrature amplitude ($\theta = 0$) can be $\hat{X}_-(\Omega) = \hat{b}(\omega_0 - \Omega) + \hat{b}^\dagger(\omega_0 + \Omega)$ and the quadrature phase ($\theta = \pi/2$) $\hat{Y}_-(\Omega) = -i[\hat{b}(\omega_0 - \Omega) - \hat{b}^\dagger(\omega_0 + \Omega)]$. The arbitrary quadrature component of the detected field can be measured by scanning the relative phase of θ. So when $\theta = 0$, the difference of the photocurrents will give the information of the quadrature amplitude of the detected field $\hat{X}_B(\Omega) = \hat{X}_-(\Omega) + g\hat{X}_+(\Omega)$, and when $\theta = \pi/2$, the quadrature phase $\hat{Y}_B(\Omega) = \hat{Y}_-(\Omega) + g\hat{Y}_+(\Omega)$.

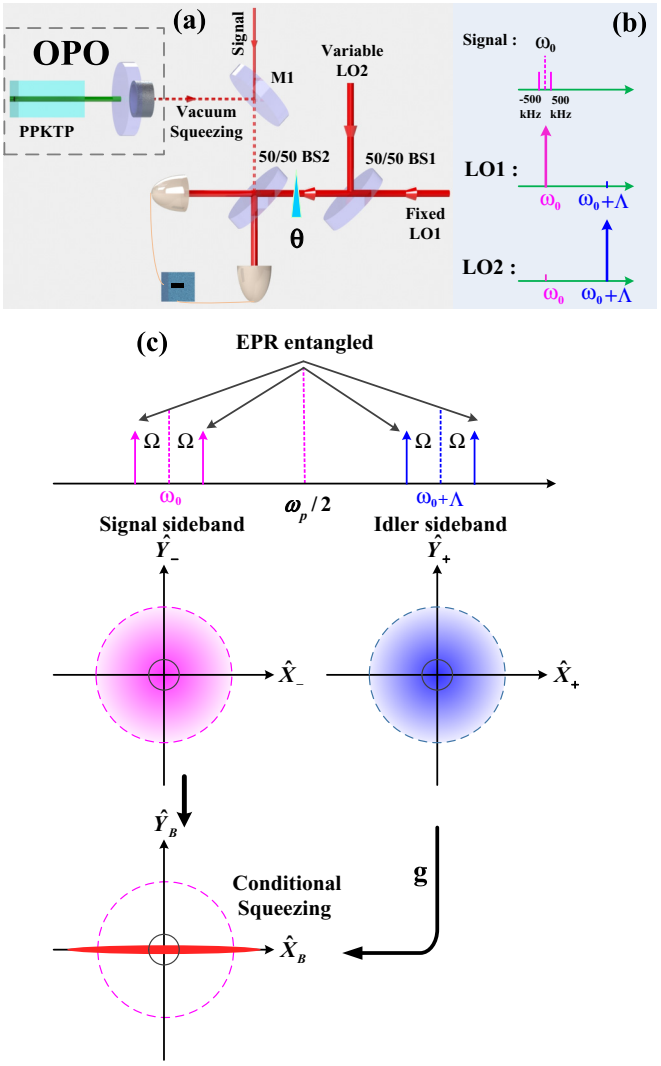

FIG. 1. The experimental setup and schematic diagram of detecting low-frequency signal beyond the standard quantum limit by a broadband squeezing and a BLO. (a) The experimental setup. OPO, optical parametric oscillator; BS, 50:50 beam splitter; LO, local oscillator; M1, 98:2 beam splitter. (b) Spectra of the weak low-frequency signal and the BLO. (c) Spectral decomposition of EPR entanglement for the broad squeezed light (upper panel) and preparation of the conditional squeezing of the signal beam by BLO detection (lower panel).

Since a single broadband squeezed light can be split into a pair of upper and lower sideband fields as EPR entangled fields, the minimum conditional variance of the output lower sideband (signal) beam can be obtained with the help of the upper sideband (idler) beam. Considering the simple OPO process, the nonlinear medium is pumped with the second-harmonic wave of $\omega_p = 2\omega_0 + \Lambda$. The annihilation operators of the output lower and upper sideband fields of an OPO can

be written as

$$\hat{b}_-^s = \hat{b}_-^0 \cosh r + \hat{b}_+^{\dagger 0} e^{i\theta_p} \sinh r,$$
$$\hat{b}_+^s = \hat{b}_+^0 \cosh r + \hat{b}_-^{\dagger 0} e^{i\theta_p} \sinh r, \quad (3)$$

where r is squeezing factor, θ_p is the phase of the pump field, and $\hat{b}_-^0$ and $\hat{b}_+^0$ are the annihilation operators of the input lower and upper sideband vacuum fields of an OPO with $\langle \delta^2 X_-^0(\Omega)\rangle = \langle \delta^2 X_+^0(\Omega)\rangle = \langle \delta^2 Y_-^0(\Omega)\rangle = \langle \delta^2 Y_+^0(\Omega)\rangle = 1$. If $\theta_p = 0$, the phase amplitudes of the output lower and upper sideband fields of an OPO can be given by

$$\hat{X}_-^s(\Omega) = \hat{X}_-^0(\Omega)\cosh r + \hat{X}_+^0(\Omega)\sinh r,$$
$$\hat{Y}_-^s(\Omega) = \hat{Y}_-^0(\Omega)\cosh r - \hat{Y}_+^0(\Omega)\sinh r,$$
$$\hat{X}_+^s(\Omega) = \hat{X}_+^0(\Omega)\cosh r + \hat{X}_-^0(\Omega)\sinh r,$$
$$\hat{Y}_+^s(\Omega) = \hat{Y}_+^0(\Omega)\cosh r - \hat{Y}_-^0(\Omega)\sinh r, \quad (4)$$

and then the difference and sum of amplitude phase quadratures of the output lower and upper sideband fields of an OPO are obtained:

$$\hat{X}_-^s(\Omega) - \hat{X}_+^s(\Omega) = [\hat{X}_-^0(\Omega) - \hat{X}_+^0(\Omega)]e^{-r},$$
$$\hat{Y}_-^s(\Omega) + \hat{Y}_+^s(\Omega) = [\hat{Y}_-^0(\Omega) + \hat{Y}_+^0(\Omega)]e^{-r},$$
$$\hat{X}_-^s(\Omega) + \hat{X}_+^s(\Omega) = [\hat{X}_-^0(\Omega) + \hat{X}_+^0(\Omega)]e^{+r},$$
$$\hat{Y}_-^s(\Omega) - \hat{Y}_+^s(\Omega) = [\hat{Y}_-^0(\Omega) - \hat{Y}_+^0(\Omega)]e^{+r}. \quad (5)$$

The variances of the output lower and upper sideband fields of an OPO are expressed by

$$\langle \delta^2 X_-^s(\Omega)\rangle = \langle \delta^2 X_+^s(\Omega)\rangle = \langle \delta^2 Y_-^s(\Omega)\rangle = \langle \delta^2 Y_+^s(\Omega)\rangle = \frac{e^{-2r} + e^{2r}}{2}, \quad (6)$$

and the correlated variances are given by

$$\langle \delta^2[\hat{X}_-^s(\Omega) - \hat{X}_+^s](\Omega)\rangle = \langle \delta^2[\hat{Y}_-^s(\Omega) + \hat{Y}_+^s(\Omega)]\rangle = 2e^{-2r},$$
$$\langle \delta^2[\hat{X}_-^s(\Omega) + \hat{X}_+^s](\Omega)\rangle = \langle \delta^2[\hat{Y}_-^s(\Omega) - \hat{Y}_+^s(\Omega)]\rangle = 2e^{+2r}. \quad (7)$$

The variance of the conditional quadrature phase $\hat{Y}_B(\Omega)$ detected by a BLO with the factor g is expressed by

$$\langle \delta^2 \hat{Y}_B(\Omega)\rangle = \langle \delta^2(\hat{Y}_-^s + g\hat{Y}_+^s)\rangle = \frac{e^{2r}}{2}(1-g)^2 + \frac{e^{-2r}}{2}(1+g)^2. \quad (8)$$

In parallel, the conditional quadrature amplitude $\hat{X}_B(\Omega)$ is given by

$$\langle \delta^2 \hat{X}_B(\Omega)\rangle = \langle \delta^2(\hat{X}_-^s + g\hat{X}_+^s)\rangle = \frac{e^{-2r}}{2}(1-g)^2 + \frac{e^{2r}}{2}(1+g)^2. \quad (9)$$

When we choose the optimized value of $g_{\rm opt} = (e^{2r} - e^{-2r})/(e^{2r} + e^{-2r})$, the minimum conditional variance of the output lower sideband field is obtained:

$$\langle \delta^2 \hat{Y}_B^{\rm opt}(\Omega)\rangle = \frac{2}{e^{2r} + e^{-2r}}. \quad (10)$$

Here the method of obtaining the minimum conditional variance by the optimized factor is the same as in previous works [37,38]. Thus, for the vacuum field injection, $g = 0$ (without the upper local oscillator $\omega_0 + \Lambda$) and $\langle \delta^2 \hat{Y}_B(\Omega)\rangle = 1$. When the broadband squeezed light with 3 dB is injected, the minimum conditional variance is -0.97 dB with $g_{\rm opt} = 0.6$.

The experimental setup and schematic diagram are shown in Fig. 1. A diode-pumped intracavity frequency-doubled single-frequency laser provides the fundamental light of 200 mW at 1064 nm and the second-harmonic light of 450 mW at 532 nm simultaneously. The second-harmonic light with the frequency of $\omega_p = 2\omega_0 + \Lambda$ is used to pump an OPO to generate the broad squeezed vacuum field. The OPO cavity is resonant for both the pump light at 532 nm and the fundamental light at 1064 nm. The OPO cavity with 38 mm long contains a type-I PPKTP crystal (1 mm × 2 mm × 10 mm), the front facet of which is highly reflective for 1064 nm and has a power transmittance of 5% for 532 nm, and an outcoupling mirror that is highly reflective at 532 nm and has an intensity transmittance of 12.5% at 1064 nm. The bandwidth of the OPO is about 70 MHz. The OPO cavity is locked by PDH (Pound-Driver-Hall) technology, and the error signal is extracted by detecting the reflected pump light of the OPO. The output broad squeezed field carries the weak low-frequency signal (±500 kHz) around the carrier frequency ω_0 at M1 (98:2 beam splitter).

The fundamental output field ($\omega_p/2$) passes through the acousto-optical frequency-shifted system and then is split into two beams with the frequency of $\omega_0 = \omega_p/2 - 5$ MHz and $\omega_0 + \Lambda = \omega_p/2 + 5$ MHz (here $\Lambda = 10$ MHz). In the frequency-shifted system, AOM1 shifts the laser frequency by the first-order diffraction with a mount of +110 MHz. Then the frequency-shifted laser is split into two parts, which are translated back by AOM2 and AOM3 with the mount of −105 MHz and −115 MHz, respectively. The two frequency-shifted laser beams at $\omega_p/2 \pm 5$ MHz as local oscillator (LO) 1 and 2 are combined on the 50:50 BS with the same polarization to generate the BLO. Here the power of LO1 is fixed and that of LO2 can be varied. A small portion from the frequency-shifted laser beams at $\omega_p/2 - 5$ MHz is used to generate the weak low-frequency signal by a phase modulator. In order to lock the relative frequency and phase of the two LOs, the signal generators of the acousto-optical frequency-shifted system are locked by the clock synchronization technology [31,33]. The squeezed light with the weak low-frequency signal is mixed with the BLO on the 50:50 BS. Finally, the two output fields of the BS are detected by two balanced detectors.

Figure 2 shows the noise variance of the conditional quadrature phase amplitude as the function of the factor g^2. Here the noise of the conditional quadrature phase amplitude is normalized to the SQL, which is determined only with the LO1 ($g = 0$) and injecting vacuum field (blocking the squeezed light and signal field). When injecting the squeezed light and given the intensity of the LO2 (given the factor of g), the conditional arbitrary quadrature components are measured by scanning the relative phase of θ. The conditional quadrature phase amplitude as the function of the factor g^2 [Fig. 2(a)] can be obtained by finding the minimum and maximum noise variance from the measured arbitrary quadrature components, which are in good agreement with the theoretical calculation.

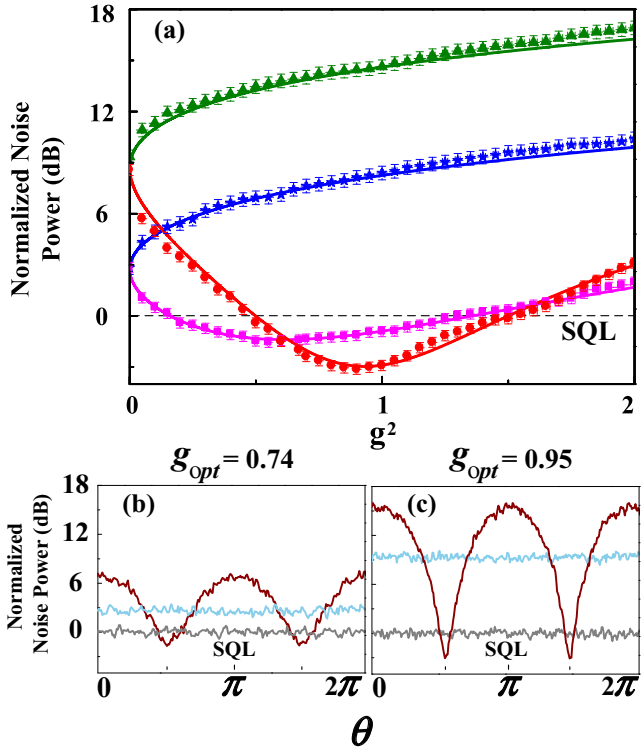

FIG. 2. The noise variance of the conditional quadrature phase amplitude. (a) The noise variance of the conditional quadrature phase amplitude as the function of the factor g^2. The conditional quadrature phase (magenta squares) and amplitude (blue stars) are for the initial squeezing, 3.9 dB (antisqueezing, 5.24 dB), and the extra noise, $N_e = 1.75$. The conditional quadrature phase (red circles) and amplitude (green triangles) are for the initial squeezing, 5.9 dB (antisqueezing, 11.6 dB), and the extra noise, $N_e = 21.1$. The solid curves are theoretical fitting according to the experimental parameters. (b) The noise variance of the conditional arbitrary quadrature components with the initial squeezing, 3.9 dB (antisqueezing, 5.24 dB), the extra noise, $N_e = 1.75$, and the optimal factor, $g_{\rm opt} = 0.74$. (c) The noise variance of the conditional arbitrary quadrature components with the initial squeezing, 5.9 dB (antisqueezing, 11.6 dB), the extra noise, $N_e = 21.1$, and the optimal factor, $g_{\rm opt} = 0.95$. The blue (light gray) curves in panels (b) and (c) are the noise variance of the arbitrary quadrature components of the lower sideband field of the squeezing light. RBW = 30 kHz, VBW = 30 Hz, and sweep time = 500 ms.

Figure 2(a) gives two different squeezing (antisqueezing) with 3.9 dB (5.24 dB) and 5.9 dB (11.6 dB), respectively. Here the extra noise N_e of the antisqueezed component can be calculated from the values of squeezing and antisqueezing (see the Appendix). Figures 2(b) and 2(c) show the noise variance of the conditional arbitrary quadrature components with the optimal factor $g_{\rm opt}$ for two different input squeezing with 3.9 dB and 5.9 dB, respectively. Thus, the minimum conditional variance is obtained with -1.5 dB for the initial squeezing of 3.9 dB and -3.1 dB for that of 5.9 dB. Here the noise variances of the arbitrary quadrature components of the lower sideband field of the squeezing light ($g = 0$) are constant and larger than SQL as the function of the relative phase of θ, which demonstrates that one beam of an EPR entangled pair is in thermal state.

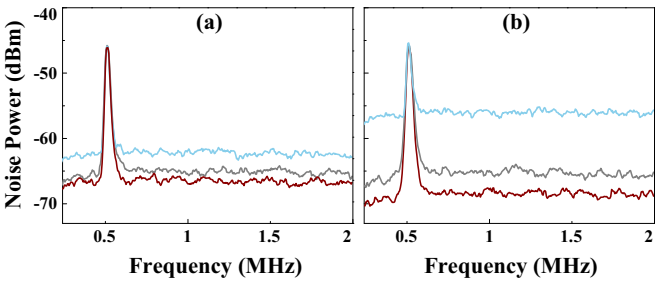

FIG. 3. The noise spectra of the low-frequency signal with 500 kHz around the frequency ω_0 by using broad squeezed light and BLO. (a) The initial squeezing is 3.9 dB ($e^{-2r} = 0.4$), and the extra noise is $N_e = 1.75$. (b) The initial squeezing is 5.9 dB ($e^{-2r} = 0.26$), and the extra noise is $N_e = 21.1$. The black (gray) curves are the noise spectrum of the signal field with the input vacuum field and $g = 0$. The blue (light gray) curves are the noise spectrum of the signal field with the input squeezed field and $g = 0$. The red (dark gray) curves are the noise spectrum of the signal field with the input squeezed field and $g_{\rm opt}$. RBW = 10 kHz, VBW = 30 Hz.

Figure 3 shows the enhanced sensitivity of low-frequency signal with 500 kHz around the frequency ω_0 by using broad squeezed light and a BLO. When the vacuum field is injected, the noise floor [black (gray) curve in Fig. 3] of the signal corresponds to SQL with $g = 0$. If the squeezed field is injected and $g = 0$, the very noisy floor [blue (light gray) curve in Fig. 3] is the noise variance of one beam of an EPR entangled pair. When we choose the optimal factor $g_{\rm opt}$, the enhanced sensitivity of the low-frequency signal is obtained, and the signal-to-noise ratio is improved with 1.5 dB for the initial broad squeezing of 3.9 dB and 3.1 dB for that of 5.9 dB. Quantum advantage resulting from the use of squeezed light is evaluated by comparing signal-to-noise ratios in this work. Because of additional degrees of freedom such as the optical gain g, a fair comparison between quantum and classical light can be difficult. However, the quantum noise floors of both the classical and the quantum approaches are compared after an independent factor over g in this work, because changing g here does not change the signal level, as evidenced in Fig. 3. In this scheme, one can avoid the low-frequency technical noise of the squeezed-light source by placing the signal and the detection in one of the squeezed sidebands. This is useful only if it is effectively the dominant source of noise. On the other hand, the low-frequency noise introduced by homodyne detection cannot be avoided in the scheme. For example, amplitude noise will be rejected by the balanced detector, up to the common-mode rejection power. However, phase noise will still creep in, particularly if the squeezing is strong.

In conclusion, we have demonstrated a scheme of using a broadband high-frequency squeezed vacuum to detect low-frequency signal beyond the standard quantum limit. By means of the EPR entanglement of the upper and lower sideband of the broadband squeezed light, the conditional variance in the low-frequency band can be obtained by BLO detection by subtracting the photocurrent of the upper sideband beam from that of the lower sideband beam. Thus this scheme does not need directly generate the squeezing in the low-frequency band. In addition, the BLO detection directly measures the signal mapped on the sideband of the squeezed state, and in this

sense this scheme can to some extent avoid the DC technical noise in the traditional homodyne detection stemming from the light sources.

ACKNOWLEDGMENTS

The authors would like to thank Yiqiu Ma for helpful discussions. This research is supported by the MOST (Grant No. 2016YFA0301602), NSFC (Grants No. 11234008, No. 11361161002, No. 11474188, No. 11654002, No. 61571276), Natural Science Foundation of Shanxi Province (Grant No. 2015011007) and the Shanxi Scholarship Council of China (Grant No. 2015-002).

APPENDIX: THE CONDITIONAL SQUEEZING WITH THE EXTRA NOISE OF THE ANTISQUEEZED COMPONENT

Usually the broadband squeezed light generated by an OPO is not the minimum uncertainty state in which the antisqueezed component has the extra noise. So the phase amplitudes of the output lower and upper sideband fields of an OPO with the extra noise can be given by

$$\begin{aligned}
\hat{X}^s_-(\Omega) &= \hat{X}^0_-(\Omega)\cosh r + \hat{X}^0_+(\Omega)\sinh r + \frac{N_X}{2},\\
\hat{Y}^s_-(\Omega) &= \hat{Y}^0_-(\Omega)\cosh r - \hat{Y}^0_+(\Omega)\sinh r + \frac{N_Y}{2},\\
\hat{X}^s_+(\Omega) &= \hat{X}^0_+(\Omega)\cosh r + \hat{X}^0_-(\Omega)\sinh r + \frac{N_X}{2},\\
\hat{Y}^s_+(\Omega) &= \hat{Y}^0_+(\Omega)\cosh r - \hat{Y}^0_-(\Omega)\sinh r - \frac{N_Y}{2},
\end{aligned} \tag{A1}$$

where $\langle\delta^2 N_X\rangle = \langle\delta^2 N_Y\rangle = N_e$. The difference and sum of amplitude phase quadratures of the output lower and upper sideband fields of an OPO are obtained:

$$\begin{aligned}
\hat{X}^s_-(\Omega) - \hat{X}^s_+(\Omega) &= [\hat{X}^0_-(\Omega) - \hat{X}^0_+(\Omega)]e^{-r},\\
\hat{Y}^s_-(\Omega) + \hat{Y}^s_+(\Omega) &= [\hat{Y}^0_-(\Omega) + \hat{Y}^0_+(\Omega)]e^{-r},\\
\hat{X}^s_-(\Omega) + \hat{X}^s_+(\Omega) &= [\hat{X}^0_-(\Omega) + \hat{X}^0_+(\Omega)]e^{+r} + N_X,\\
\hat{Y}^s_-(\Omega) - \hat{Y}^s_+(\Omega) &= [\hat{Y}^0_-(\Omega) - \hat{Y}^0_+(\Omega)]e^{+r} + N_Y.
\end{aligned} \tag{A2}$$

The variances of the output lower and upper sideband fields of an OPO are expressed by

$$\begin{aligned}
\langle\delta^2 X^s_-(\Omega)\rangle &= \langle\delta^2 X^s_+(\Omega)\rangle = \langle\delta^2 Y^s_-(\Omega)\rangle = \langle\delta^2 Y^s_+(\Omega)\rangle\\
&= \frac{e^{-2r}+e^{2r}}{2} + \frac{N_e}{4},
\end{aligned} \tag{A3}$$

and the correlated variances are given by

$$\begin{aligned}
\langle\delta^2[\hat{X}^s_-(\Omega) - \hat{X}^s_+](\Omega)\rangle &= \langle\delta^2[\hat{Y}^s_-(\Omega) + \hat{Y}^s_+(\Omega)]\rangle = 2e^{-2r},\\
\langle\delta^2[\hat{X}^s_-(\Omega) + \hat{X}^s_+](\Omega)\rangle &= \langle\delta^2[\hat{Y}^s_-(\Omega) - \hat{Y}^s_+(\Omega)]\rangle\\
&= 2e^{+2r} + N_e.
\end{aligned} \tag{A4}$$

The variance of the conditional quadrature phase $\hat{Y}_B(\Omega)$ and amplitude $\hat{X}_B(\Omega)$ detected by the BLO with a factor are expressed by

$$\begin{aligned}
\langle\delta^2\hat{Y}_B(\Omega)\rangle &= \langle\delta^2(\hat{Y}^s_- + g\hat{Y}^s_+)\rangle\\
&= \frac{1}{2}\left(e^{2r} + \frac{N_e}{2}\right)(1-g)^2 + \frac{e^{-2r}}{2}(1+g)^2,\\
\langle\delta^2\hat{X}_B(\Omega)\rangle &= \langle\delta^2(\hat{X}^s_- + g\hat{X}^s_+)\rangle\\
&= \frac{1}{2}\left(e^{2r} + \frac{N_e}{2}\right)(1+g)^2 + \frac{e^{-2r}}{2}(1-g)^2.
\end{aligned} \tag{A5}$$

When we choose the optimized value of $g_{\rm opt} = (e^{2r} + N_e/2 - e^{-2r})/(e^{2r} + N_e/2 + e^{-2r})$, the minimum conditional variance of the output lower sideband field is obtained:

$$\left\langle\delta^2\hat{Y}^{\rm opt}_B(\Omega)\right\rangle = \frac{2e^{-2r}(e^{2r} + N_e/2)}{e^{2r} + N_e/2 + e^{-2r}}. \tag{A6}$$

At the same time, we may give the quadrature amplitude $\hat{Y}_B(\Omega)$ with the same condition expressed by

$$\begin{aligned}
\langle\delta^2\hat{X}_B(\Omega)\rangle &= \langle\delta^2(\hat{Y}^s_- + g\hat{Y}^s_+)\rangle\\
&= \frac{1}{2}\left(e^{2r} + \frac{N_e}{2}\right)(1-g)^2 + \frac{e^{-2r}}{2}(1+g)^2.
\end{aligned} \tag{A7}$$

[1] B. P. Abbott (LIGO Scientific Collaboration and the Virgo Collaboration), Phys. Rev. Lett. **116**, 061102 (2016).
[2] B. P. Abbott *et al.* (LIGO Scientific Collaboration and the Virgo Collaboration), Phys. Rev. Lett. **116**, 131102 (2016).
[3] B. P. Abbott *et al.* (LIGO Scientific Collaboration and the Virgo Collaboration), Phys. Rev. Lett. **116**, 131103 (2016).
[4] C. M. Caves, Phys. Rev. D **23**, 1693 (1981).
[5] M. Xiao, L.-A. Wu, and H. J. Kimble, Phys. Rev. Lett. **59**, 278 (1987).
[6] P. Grangier, R. E. Slusher, B. Yurke, and A. LaPorta, Phys. Rev. Lett. **59**, 2153 (1987).
[7] LIGO Scientific Collaboration, Nat. Phys. **7**, 962 (2011).
[8] LIGO Scientific Collaboration, Nat. Photonics **7**, 613 (2013).
[9] H. J. Kimble, Y. Levin, A. B. Matsko, K. S. Thorne, and S. P. Vyatchanin, Phys. Rev. D **65**, 022002 (2001).
[10] S. Chelkowski, H. Vahlbruch, B. Hage, A. Franzen, N. Lastzka, K. Danzmann, and R. Schnabel, Phys. Rev. A **71**, 013806 (2005).
[11] J. Laurat, T. Coudreau, G. Keller, N. Treps, and C. Fabre, Phys. Rev. A **70**, 042315 (2004).
[12] C. F. McCormick, A. M. Marino, V. Boyer, and P. D. Lett, Phys. Rev. A **78**, 043816 (2008).
[13] T. Horrom, R. Singh, J. P. Dowling, and E. E. Mikhailov, Phys. Rev. A **86**, 023803 (2012).
[14] N. Otterstrom, R. C. Pooser, and B. J. Lawrie, Opt. Lett. **39**, 6533 (2014).
[15] R. C. Pooser and B. J. Lawrie, ACS Photonics **3**, 8 (2016).

[16] W. J. Fan, B. J. Lawrie, and R. C. Pooser, Phys. Rev. A **92**, 053812 (2015).
[17] A. Huck, S. Smolka, P. Lodahl, A. S. Sørensen, A. Boltasseva, J. Janousek, and U. L. Andersen, Phys. Rev. Lett. **102**, 246802 (2009).
[18] M. W. Holtfrerich, M. Dowran, R. Davidson, B. J. Lawrie, R. C. Pooser, and A. M. Marino, Optica **3**, 985 (2016).
[19] R. C. Pooser and B. Lawrie, Optica **2**, 393 (2015).
[20] U. B. Hoff, G. I. Harris, L. S. Madsen, H. Kerdoncuff, M. Lassen, B. M. Nielsen, W. P. Bowen, and U. L. Andersen, Opt. Lett. **38**, 1413 (2013).
[21] J. D. Teufel, T. Donner, M. A. Castellanos-Beltran, J. W. Harlow, and K. W. Lehnert, Nat. Nanotechnol. **4**, 820 (2009).
[22] V. Boyer, A. M. Marino, and P. D. Lett, Phys. Rev. Lett. **100**, 143601 (2008).
[23] B. J. Lawrie and R. C. Pooser, Opt. Express **21**, 7549 (2013).
[24] M. I. Kolobov and C. Fabre, Phys. Rev. Lett. **85**, 3789 (2000).
[25] J. Zhang, Phys. Rev. A **67**, 054302 (2003).
[26] E. H. Huntington, G. N. Milford, C. Robilliard, T. C. Ralph, O. Glöckl, U. L. Andersen, S. Lorenz, and G. Leuchs, Phys. Rev. A **71**, 041802(R) (2005).
[27] B. Hage, A. Samblowski, and R. Schnabel, Phys. Rev. A **81**, 062301 (2010).
[28] Y. Ma, H. Miao, B. H. Pang, M. Evans, C. Zhao, J. Harms, R. Schnabel, and Y. Chen, arXiv:1612.06934.
[29] A. M. Marino, C. R. Stroud, V. Wong, R. S. Bennink, and R. W. Boyd, J. Opt. Soc. Am. B **24**, 335 (2007).
[30] H. Fan, D. He, and S. Feng, J. Opt. Soc. Am. B **32**, 2172 (2015).
[31] W. Li, X. Yu, Z. Meng, Y. Jin, and J. Zhang, Sci. China-Phys. Mech. Astron. **58**, 104201 (2015).
[32] J.-B. Béguin, E. M. Bookjans, S. L. Christensen, H. L. Sørensen, J. H. Müller, E. S. Polzik, and J. Appel, Phys. Rev. Lett. **113**, 263603 (2014).
[33] W. Li, X. Yu, and J. Zhang, Opt. Lett. **40**, 5299 (2015).
[34] W. Li, Y. Jin, and X. Yu, Sci. China-Phys. Mech. Astron. **60**, 050321 (2017).
[35] M. Pysher, Y. Miwa, R. Shahrokhshahi, R. Bloomer, and O. Pfister, Phys. Rev. Lett. **107**, 030505 (2011).
[36] O. Pinel, P. Jian, R. M. de Araújo, J. Feng, B. Chalopin, C. Fabre, and N. Treps, Phys. Rev. Lett. **108**, 083601 (2012).
[37] M. D. Reid, Phys. Rev. A **40**, 913 (1989).
[38] A. M. Marino, R. C. Pooser, V. Boyer, and P. D. Lett, Nature (London) **457**, 859 (2009).